Engineered SH3-Derived Sherpabodies Function as a Modular Platform for Targeted T-cell Immunotherapy

Rogelio A. Hernández-López[1], Tapio Kesti[2], Anna R. Mäkelä[2], Zhe Zhao[2], Wei Yu[1], Yurie Tonai[1], Hector J. Monzo[3], Kerttu Kalander[3,4], Sirpa Leppä[4,5,6], Päivi M. Ojala[3,6], Wendell A. Lim[1], and Kalle Saksela[2,7]

ABSTRACT

Engineered T-cell therapies have emerged as a promising approach for cancer treatment, yet their application to solid tumors remains challenging because of the limited specificity and persistence of current antigen recognition strategies. In this study, we introduce sherpabodies, engineered from a human SH3 domain scaffold, as a class of antibody-mimetic proteins capable of precise tumor-associated antigen (TAA) recognition. A phage display library identified sherpabodies against a panel of popular TAAs, which were subsequently incorporated into second-generation chimeric antigen receptor (CAR) constructs that were termed sherpabody-guided CARs (SbCAR). These SbCARs demonstrated potent *in vitro* specificity and cytotoxicity against solid cancer TAAs, without cross-reactivity to closely related proteins. The modularity, versatility, and small size of sherpabodies enabled generation of multispecific SbCARs, in particular trispecific SbCARs with OR logic that could robustly activate with cells expressing any or combinations of three cognate TAA targets, as well as circuits with IF–THEN logic in combination with synthetic Notch. *In vivo*, SbCAR T cells elicited a dose-dependent antitumor response in xenograft mouse models, highlighting their potential for therapeutic application. Furthermore, an inducible SbCAR system displayed enhanced persistence and antitumor activity when compared with constitutive CARs. These findings suggest that sherpabodies represent a versatile and promising platform for the next generation of CAR T-cell therapies, particularly for solid tumors.

Significance: Sherpabodies represent a biological targeting technology that could help extend the success of CAR T-cell therapy from treating leukemias and lymphomas to the treatment of solid cancers.

Introduction

The landscape of therapeutics for oncology is undergoing a significant transformation with the development of immunotherapies. Engineered T cells, particularly those equipped with chimeric antigen receptors (CAR), are gaining attention, demonstrating unprecedented efficacy in targeting malignancies through a mechanism that bypasses traditional MHC-dependent immune recognition. Central to the CAR modality is the extracellular antigen-targeting domain, often a single-chain variable fragment (scFv), which is bridged by a membrane-spanning peptide to intracellular domains essential for T-cell activation, proliferation, and cytotoxicity (1).

Although the clinical success of CAR T-cell therapies, particularly in hematologic malignancies targeting CD19 and B-cell maturation antigen (BCMA), is undeniable (2, 3), their translation to solid tumors has been slower. Challenges include the scarcity of truly cancer-specific antigens that would allow precise targeting of malignant but not normal cells. Tumor-associated antigens (TAA) are expressed at lower levels also in normal tissues, leading to cases of toxic cross-reactivity when these antigens are targeted by CAR T cells (4). Advances in computational analysis and synthetic biology are beginning to address these issues by enabling the design of multispecific receptors and regulatory circuits that use combinatorial antigen signatures (5–10).

A promising avenue in improving the specificity and efficacy of CAR T cells against solid tumors lies in the engineering of smaller and specific antigen-binding domains. For example, nanobodies, derived from camelid antibodies, contain one heavy chain variable region and offer comparable binding affinities to scFvs with a fraction of the size (11, 12). Various cancers are being targeted by nanobody-based CAR T cells for treating both hematologic and solid tumors (13, 14). These smaller recognition domains are advantageous to reduce the overall genetic payload that has to be accommodated by limited total capacity of gene transfer vectors used in cell therapy. This requirement is increased by the need also to overcome the immunosuppressive tumor microenvironment, counteract T-cell exhaustion, and enhance tumor infiltration, all challenges that may require additional genetic modifications to the T-cell therapy and demand for additional genetic payload.

[1]Department of Cellular and Molecular Pharmacology, Cell Design Institute, University of California San Francisco, San Francisco, California. [2]Department of Virology, University of Helsinki, Helsinki, Finland. [3]Translational Cancer Medicine Research Program, Faculty of Medicine, University of Helsinki, Helsinki, Finland. [4]Applied Tumor Genomics Research Program, Faculty of Medicine, University of Helsinki, Helsinki, Finland. [5]Department of Oncology, Helsinki University Hospital Comprehensive Cancer Center, Helsinki, Finland. [6]iCAN Digital Precision Cancer Medicine Flagship, Helsinki, Finland. [7]HUS Diagnostic Centre, HUSLAB, Clinical Microbiology, Helsinki University Hospital, Helsinki, Finland.

Current address for R.A. Hernández-López: Department of Bioengineering, Department of Genetics, Stanford University, California and Chan-Zuckerberg Biohub - San Francisco, San Francisco, California; and current address for Z. Zhao: Departments of Laboratory Medicine and Immunobiology, Yale School of Medicine, New Haven, Connecticut.

Corresponding Authors: Rogelio A. Hernández-López, James H. Clark Center, Stanford University, 318 Campus Drive, Stanford, CA 94305. E-mail: rogelioh@stanford.edu; Wendell A. Lim, UCSF, MC 2240, Genentech Hall Room N414, 600 16th Street, San Francisco, CA 94158-2517. E-mail: wendell.lim@ucsf.edu; and Kalle Saksela, University of Helsinki, PO Box 21, Helsinki 00014, Finland. E-mail: kalle.saksela@helsinki.fi

Cancer Res 2025;85:1874–87

doi: 10.1158/0008-5472.CAN-24-1959

In this context, we introduce sherpabodies, a novel class of antibody-mimetic proteins engineered from a highly optimized human nephrocystin 1 (NPHP1) SH3 domain scaffold in which six random amino acid residues have been introduced in place of its two specificity-determining loop regions (see **Fig. 1A**; ref. 15). Sherpabodies are notably compact, approximately 60 amino acids in length, and exhibit a robust thermostability. We developed the sherpabody platform building on earlier generations of SH3 scaffolds, including Fynomers, for which manipulation of the corresponding loop regions has been shown to confer the ability to target cytokines (16), viral proteins (15, 17), and tumor vascular structures (18), showing the adaptability and potential of this approach in therapeutic contexts.

Here, we report the integration of sherpabodies into CARs [sherpabody-guided CARs (SbCAR)], leveraging a high-throughput platform to tailor T cells with precise targeting capabilities against a variety of TAAs. We demonstrate their potent cytotoxic activity both *in vitro* and in xenograft cancer models. Our results underscore the potential of SbCARs in immunotherapy, particularly for solid tumors, facilitated by the intrinsic modularity of sherpabodies, which supports the construction of multispecific receptors and regulatory circuits. This study provides a modular and specific targeting platform that might overcome the current challenges in treating solid tumors and offers a promising strategy for the development of next-generation CAR T therapies.

Materials and Methods

Phage panning

A sherpabody phage display library (size ~1 x 10^{11} cfu) was obtained from Next Biomed Therapies Oy. Screening and characterization of novel sherpabody-displaying phages targeted against selected tumor-associated surface antigens were performed as previously described (15). Specific phage-displayed sherpabodies were selected by panning against immobilized TAAs (30 μg/mL in PBS; MaxiSorp Immunotubes, Nunc), HER2 (HE2-H5253, lot 263-6ACF1-CU), FOLR1 (FO1-H253, lot 2773b-935F1-MV), EpCAM (EPM-H5254, lot 144-88HF1-KG), HER3 (ER3-H5259, lot 219-218KF1-KP), TROP2 (TR2-H5253, lot 3529A-20AMF1-135), human IgG1 Fc (hIgG1Fc) or EphA2-His (EP2-H52H4, lot 595b-2241F1-13A) fusion proteins (all from ACROBiosystems), and an hFc control protein (trastuzumab).

Screening and characterization of specific sherpabody clones by ELISA

Representative transformants from the second and third panning rounds were tested for specific binding to the extracellular domains of tumor-associated target antigens and an hIgG1Fc control protein by ELISA as previously described (15). The DNA encapsulated by the positive phage clones was then sequenced and translated to determine the sequence of the displayed sherpabody. Semiquantitative phage-ELISA was used to determine the relative binding strength (strong vs. moderate) of each unique sherpabody to its immobilized target antigen. To allow comparison, the quantity of each sherpabody-displaying phage clone was normalized using the interaction of sherpabody-fused E-tag and rabbit polyclonal E-tag antibody (GE HealthCare; 27941201V; lot 355351) as a reference signal. Antigen cross-reactivity was investigated by phage-ELISA using phage stocks diluted 1:1 in 5% milk-PBS (100 μL per well) and immobilized target antigens (2 μg/mL): HER2, FOLR1, EpCAM, HER3, TROP3, EphA, and a control protein EGFR (EGR-H5252, lot 262-91Xf1-PE, ACROBiosystems). The ELISA was performed using standard protocols as earlier described (15). Polyreactivity ELISA was used to evaluate nonspecific binding of sherpabody-displaying phages (1:1 in 5% milk-PBS) to a panel of promiscuously interacting macromolecules (19, 20), namely, cardiolipin (50 μg/mL; C0563, lot SLCC2621, Sigma), keyhole limpet hemocyanin (5 μg/mL; H8283, Sigma), lipopolysaccharide (10 μg/mL; L2630-10MG, lot 000011516, Sigma), ssDNA (1 μg/mL; D8899, lot SLCC4481, Sigma), double-stranded DNA (1 μg/mL; D4522, lot SLCD4909 Sigma), insulin (1 μg/mL; 91077C-100MG, lot 21C053, SAFC), and an anti–E-tag antibody. The ELISA was essentially performed as previously described with the exception that 2.5% milk-PBS was used as a blocking buffer throughout the protocol (15).

Sherpabody production and purification

Selected sherpabodies were cloned and expressed in *Escherichia coli* as GST-fusion proteins using standard protocols (GE HealthCare). A 15-mer Gly-Ser, (GGGGS)3 linker was introduced in between the sherpabody and GST and a biotin acceptor peptide (GLNDIFEAQKIEWHE) into the C-terminus of each fusion protein. The *in vivo* biotinylated sherpabodies were produced in the RV308 bacterial strain in the presence of BirA ligase and D-biotin (50 μmol/L; Sigma). The fusion proteins were purified by affinity chromatography using glutathione sepharose according to the manufacturer's instructions (GE HealthCare). The buffer was exchanged to PBS by dialysis (140 mmol/L NaCl, 10 mmol/L phosphate buffer, and 3 mmol/L KCl, pH 7.4), and the purified sherpabodies were stored at −80°C and/or at +4°C.

Affinity analysis by biolayer interferometry

Affinity measurements were performed by biolayer interferometry using the Octet Red384 system (FortéBio). The biotinylated binders (Sb1205, Sb1322, and Sb1324) were immobilized on streptavidin biosensors (FortéBio) for 1 minute at 5 μg/mL in a kinetics buffer (Sartorius). The final immobilization level was ~2 nm. Binding of the analyte (Her2-His, HE2-H5225, lot C49P1-20B3F1-VK, ACROBiosystems) diluted in the kinetics buffer at various concentrations was then measured using association and dissociation periods of 5 minutes. The reference sample data (0 nmol/L) were subtracted. The data were fitted with a model of "one-to-one binding."

Gene synthesis and cloning

TAA sherpabodies: Genes encoding sherpabody variants were obtained by gene synthesis as gBlocks (Integrated DNA Technologies). Gene fragments were codon-optimized for expression in human cells using Integrated DNA Technologies' website tool. Similarly, genes encoding anti-HER2 scFv were obtained by gene synthesis as gBlocks (Integrated DNA Technologies). All constructs were built via in-fusion cloning (Clontech #ST0345) and sequence-verified before using them.

CAR, synthetic Notch receptor, and response element construct design

Sherpabody CARs were built by fusing the recognition domain to the hinge region of the human CD8α chain and transmembrane and cytoplasmic regions of the human 4-1BB and CD3z signaling domains. CARs were expressed under the control of a spleen focus-forming virus promoter. Constitutive and inducible CAR constructs contain an N-terminal 3X Flag-tag and C-terminal mCherry protein to determine their protein expression levels. An anti-HER2

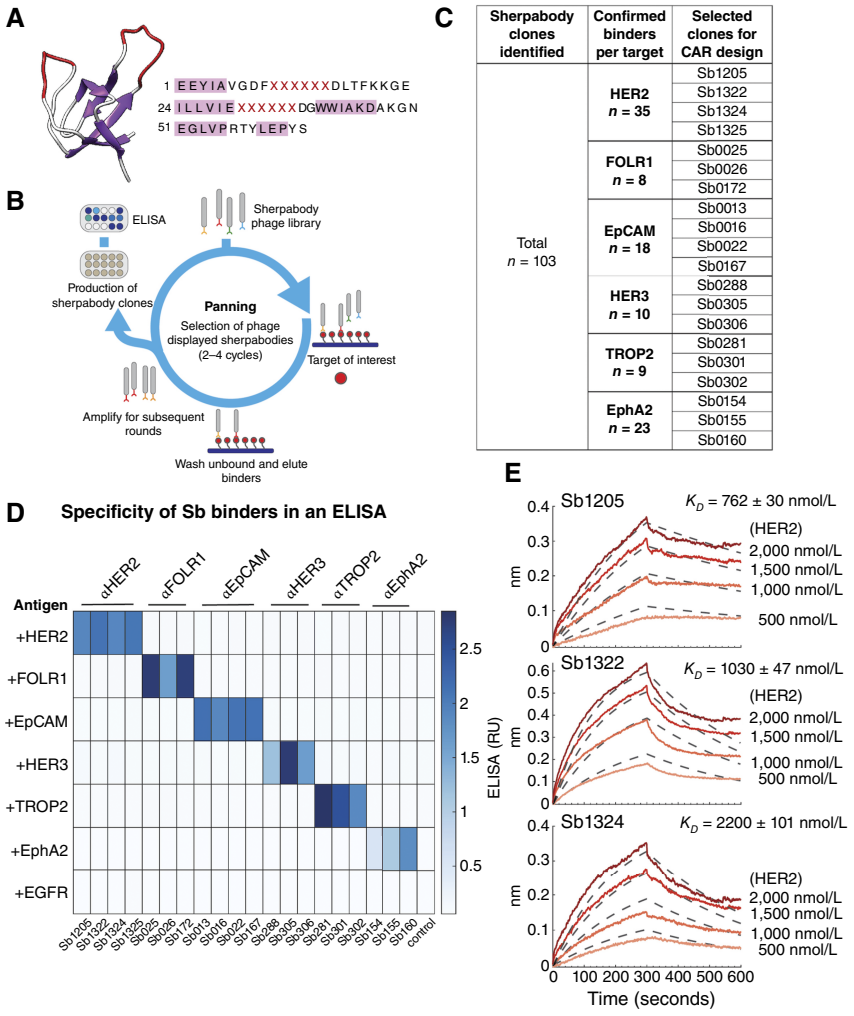

Figure 1.

Platform for selection and characterization of sherpabodies targeted against common TAAs in solid tumors. **A,** Structure of the sherpabody made of 60 amino acids engineered from a human NPHP1 SH3 domain scaffold. The five β-strands giving rise to its β-barrel fold are indicated in purple. The sequences containing random hexamer sequences that replaced six and three NPHP1 residues in the loop regions before and after, respectively, the second β-strand are shown in red. **B,** Schematic of the sherpabody selection strategy combining phage panning against immobilized TAAs. Three or four rounds of selection yielded high-affinity sherpabody clones that were sequenced and further characterized by ELISA. **C,** Selection of 20 sherpabody clones obtained from the biopanning procedure that were further evaluated. **D,** Semiquantitative phage-ELISA of each sherpabody (Sb) to the panel of immobilized TAAs. Data were normalized using the interaction of sherpabody-fused E-tag and rabbit polyclonal E-tag antibody. **E,** Binding affinities for anti-HER2 sherpabodies as determined by biolayer interferometry. Sensograms show the binding kinetics for human HER2 and immobilized anti-HER2 sherpabodies. Data are shown as colored traces, and the best fit for data to a 1:1 model is shown in dashed lines. The HER2 concentrations used for the binding affinity measurements are indicated.

synthetic Notch (synNotch) receptor of a low affinity (210 nmol/L) contains anti-HER2 scFv fused to the mouse Notch1 minimal regulatory region followed by a Gal4 DNA-binding domain and the VP64 activation domain, as previously described (8, 21, 22). The synNotch receptor contains an N-terminal CD8α signaling peptide (MALPVTALLLPLALLLHAARP) for membrane targeting and a myc-tag (EQKLISEEDL) for determination of surface expression levels. The synNotch to SbCAR circuit construct was cloned into a single plasmid to avoid copy-number variability as previously described (22). The anti-HER2 scFv recognition domain sequences have been previously described (22, 23).

Cancer cell lines

Target cells were cultured to confluence in the indicated media supplemented with 10% FBS. For passaging, cells were washed with warmed PBS, and then, TrypLE (Thermo Fisher Scientific 12604021) was added to detach the cells from the flask surface. Flasks were incubated at 37°C until the cells detached, typically 5 to 10 minutes. A fresh culture medium with FBS was added to quench the TrypLE, and cells were resuspended and plated in new flasks and in fresh culture medium. The following cancer cell lines were purchased from the indicated vendors and cultured in the indicated media: PC3 cells (ATCC CRL-1435, RRID: CVCL_0035) were cultured in F-12K medium; SKOV3 cells (ATCC CRL-HTB77, RRID: CVCL_0532) in McCoy's 5A medium; and HeLa (ATCC CCL-2, RRID: CVCL_0030), 293T (ATCC CRL-3216, RRID: CVCL_0063), and BT474 cells (ATCC CRL-HTB20, RRID: CVCL_0179) in RPMI medium. HCC1569 (RRID: CVCL 1255) cell lines were gifts from the Moasser lab [University of California San Francisco (UCSF)] and cultured in RPMI medium. We did not passage the cell lines for more than 10 times after revival from frozen stocks, did not subject them to further authentication, and tested all active cultures bimonthly with MycoAlert PLUS Mycoplasma Detection Kit (Lonza).

HER2 expression in 293T, PC3, and HeLa cell lines was downregulated by lentiviral short hairpin RNA (shRNA) silencing. Lentiviral plasmids encoding shRNAs that target HER2 (TRCN0000010342 for PC3 and HeLa; TRCN0000039878 for 293T cells) were obtained from the Sigma-Aldrich MISSION shRNA library, distributed by the Genome Biology Unit core facility supported by HiLIFE and the Faculty of Medicine, University of Helsinki, and Biocenter Finland.

Expression of TAAs in target cell lines

For detection of TAAs, the following antibodies were used: mouse anti-EpCAM (sc-25308, lot H1021, Santa Cruz Biotechnology, RRID: AB_627531), mouse anti-FOLR1 (MAB5646, lot

CCQX0819121, R&D Systems, RRID: AB_2278620), anti-HER2 (trastuzumab, lot F2003025, Samsung Bioepis), goat anti–mouse IgG-Alexa Fluor 488 (A11001, lot 2247988, Invitrogen), and goat anti–human IgG-DyLight488 (SA5-10134, lot WE3282739, Invitrogen). Exponentially growing cells were washed with PBS and detached with 3 mmol/L EDTA/PBS. A total of 200,000 cells were stained using the primary antibodies diluted in FACS buffer at 4°C for 30 minutes. After washing twice with FACS buffer, cells were stained with fluorescently labeled secondary antibodies diluted in FACS buffer at 4°C for 30 minutes. The cells were washed once with FACS buffer and analyzed with a BD LSRFortessa flow cytometer. Cells stained only with the secondary antibodies were used as negative controls.

In vitro activation assay using J-CAR T cells

To generate J-CAR T cells, Jurkat reporter T cells (24) were transduced with lentiviruses expressing sherpabody-based CAR proteins fused to mCherry. After 20 to 24 hours, cells were collected by centrifugation, washed once with RPMI medium, and subjected to the following activation assays: For activation with purified proteins, C96 MaxiSorp plates (446612, lot 172565, Thermo Fisher Scientific) were coated with soluble recombinant proteins (40 μg/mL of EpCAM and 20 μg/mL of other proteins in PBS) overnight at 4°C, and washed twice with PBS and once with RPMI medium. To test CAR activation with transfected proteins, pEBB-expression plasmids with cDNAs encoding human FOLR1, EpCAM, and HER2 were transfected into 293T cells. Twenty-four hours later, cells were detached with trypsin treatment and plated on a 96-well plate. Cancer cells expressing targeted antigens were plated in a similar manner to 80% confluence. J-CAR T cells were added to each of the wells, and the plates were centrifuged at 400 × *g* for 1 minute and were incubated for 20 to 24 hours. Then J-CAR T cells were fixed in 2% paraformaldehyde for 20 minutes, washed with FACS buffer, and transferred into FACS tubes, and expression of EGFP and ECFP in mCherry-positive cells was measured with a flow cytometer (BD LSRFortessa). Data were analyzed using FlowJo software (v. 10, BD Biosciences, RRID: SCR_008520).

Engineered K562-HER2 cell lines

Engineered K562-HER2 cell lines were subcultured in Iscove's Modified Dulbecco's Medium supplemented with 10% FBS and gentamicin as previously described (22). The HER2 levels in each target cell have been previously described in Hernandez-Lopez and colleagues.

Primary human T-cell isolation and culture

Primary $CD4^+$ and $CD8^+$ T cells were isolated from the blood of anonymous donors obtained under approvals of local review boards from blood centers (Finnish Red Cross or the Pacific) by negative selection (STEMCELL Technologies #15062 and #15063). T cells were cryopreserved in RPMI-1640 (UCSF cell culture core) with 20% human AB serum (Valley Biomedical, #HP1022) and 10% DMSO. T cells were cultured in human T-cell medium consisting of X-VIVO 15 (Lonza #04-418Q), 5% human AB serum, and 10 mmol/L neutralized N-acetyl L-cysteine (Sigma-Aldrich #A9165) supplemented with 30 U/mL IL2 (NCI BRB Preclinical Repository) for all experiments.

Lentiviral transduction of human T cells

Pantropic VSV-G pseudotyped lentivirus was produced by transfecting Lenti-X 293T cells (Clontech #11131D) with a transgene expression vector and the viral packaging plasmids pCMV-dR8.91 and pMD2.G using FuGENE HD (Promega #E2312). Primary T cells were thawed, and after 24 hours in culture, were stimulated with Human T-Activator CD3/CD28 DynaBeads (Life Technologies #11131D) at a 1:1 cell:bead ratio. After 48 hours, the viral supernatant was harvested and added to primary T cells. T cells were exposed to the virus for 24 hours. At day 5, after T-cell stimulation, the DynaBeads were removed. T cells were stained and sorted on an BD FACSAria Fusion cell sorter (BD Biosciences) on the basis of mCherry to obtain homogeneous CAR expression levels. For the single vector containing the synNotch to CAR circuit, T-cell transduction efficiency ranged between 10% and 30%, indicating that a single copy of the circuit was inserted. More than 90% of T cells did not express CAR, but the few that did (leaky expression) were removed by cell sorting. Untransduced T cells were used to set up the sorting gates but were not sorted as engineered T cells. T cells were expanded for at least 9 days and cultured at 0.5 million/mL when they were rested and were used for killing assays.

Determination of *in vitro* cytotoxicity with a luciferase reporter

Target cells were engineered to constitutively express Renilla luciferase by lentiviral transduction. A total of 10,000 cells were plated in triplicate in ViewPlate-96 F TC plates (6005182, PerkinElmer), and mCherry-positive CAR T cells were added at the indicated ratios. On average, 30% of CAR T cells were mCherry positive, and this estimate was used for untransduced (mock) T cells. After coculturing in an incubator for 72 hours at 37°C and 5% CO_2, the remaining luciferase activity was measured using the Renilla-Glo luciferase assay system (E2720, Promega) and Promega GloMax Navigator microplate luminometer.

Measurement of cytokine responses

Cytokine secretion was induced by coculturing (primary) CAR T cells and target cells as previously described (25). The IL2 and IFNγ cytokine expression levels were quantified from the coculture supernatants by ELISA according to the manufacturer's instructions (Thermo Fisher Scientific #88-7025-88 and #88-7316-88, respectively). The samples were calibrated and concentrations estimated using the protein standard curves. Average and SD of three parallel experiments are shown.

Determination of K562-HER2 *in vitro* T-cell cytotoxicity

$CD8^+$ primary human T cells expressing constitutive anti-HER2 SbCAR (1205) were cocultured for 72 hours with targets expressing different HER2 densities in a complete human T-cell medium and placed in an incubator at 37°C and 5% CO_2. In all *in vitro* T-cell killing assays against engineered K562-HER2 cells, the T cells were cocultured in round-bottom 96-well tissue culture plates at the indicated effector-to-target (E:T) ratios. The cells were centrifuged for 1 minute at 400 × *g* to favor E:T interactions, and the cultures were analyzed after 3 days for specific lysis of target tumor cells by flow cytometry. The percentage of specific lysis of target cells was determined by comparing the number of target cells alive in the coculture with engineered T cells compared with treatment with untransduced T-cell controls. All flow cytometry was performed using BD LSRII (RRID: SCR_002159) or Attune NxT (RRID: SCR_019590) flow cytometers. We used the recommended conditions for accurate cell counting in terms of flow rates (100 μL/minute), sample volume (50 μL), and event rates (<8,000 events/second). The analysis was performed in FlowJo software (TreeStar, RRID:

SCR_008520) and MATLAB (RRID: SCR_001622). The following equation was used to calculate the percent of specific lysis:

$$\%\ specific\ lysis = \left(1 - \frac{Live\ Targets\ in\ coculture\ with\ engineered\ Tcells}{Live\ Targets\ in\ coculture\ with\ UnT\ T\ cells}\right) \times 100$$

Human T-cell phenotyping of SbCARs

T-cell differentiation states were assessed using the following antibodies: BV605 anti-CD45RA (clone HI100, #304133, BioLegend, RRID: AB_11126164) and allophycocyanin–Cy7 anti-CD62L (clone DREG-56, #304813, BioLegend, RRID: AB_493583). Briefly, post-transduced inducible and constitutive SbCAR T cells (Sb1205) were sorted, expanded, and rested for about 10 days and then analyzed by flow cytometry. To assess the influence of antigen-dependent activation on the T-cell phenotype, T cells from four independent donors were cocultured at an E:T ratio of 1:1 (25,000:25,000) for 72 hours with target K562-HER2 (high) cells. We used a 1:100 antibody dilution. A total volume of 50 μL per staining reaction was used in staining buffer (PBS with 2% FBS). Samples were incubated at 4°C for 30 minutes and washed with staining buffer. T cells were analyzed by flow cytometry in LSRFortessa (BD Biosciences), and the analysis was performed in FlowJo software (TreeStar).

In vivo tumor killing and mouse models

All mouse experimental procedures were conducted following UCSF Institutional Animal Care and Use Committee–approved protocols. Female NOD/SCID gamma mice were obtained from the UCSF breeding core. Six- to 12- week-old animals were inoculated with tumor-cell suspensions in PBS mixed 1:1 with Matrigel (Corning). Three million in 50 μL were inoculated subcutaneously in the right (high density) and left (low density) flanks, or right-only flank for single-tumor experiments. Single-dose treatments consisting of sorted and rested $CD4^+$ and $CD8^+$ (donor matched) engineered or the same number of untransduced T cells were administered intravenously via tail vein in 100 μL of PBS at day 28 (for double tumor) or day 37 (single tumor) after tumor injection. Animals were randomized at the moment of T-cell injection, and the median tumor volume was ~100 mm^3. Tumor volumes were monitored once a week via caliper measurements until predetermined The institutional animal care and use committee–approved endpoint (hunching and neurologic impairments such as circling, ataxia, paralysis, limping, head tilt, balance problems, seizures, and tumor volume burden) was reached (n = 5–9 mice per group). Statistical longitudinal analyses were performed over entire segments of the tumor growth curves using TumGrowth. This analysis includes automatic analyses of breakpoints in the tumor growth and outlier detection using Bonferroni-corrected P values calculated from the residuals. The tumor growth curves were subjected to type II ANOVA and pairwise comparisons across groups, and the P values are reported without and with adjustment by the Holm method.

In vivo luciferase imaging of SbCAR T cells

Primary human T cells were engineered to constitutively express effLuc and the SbCAR construct. T-cell localization was measured after 2 days of intravenous injections and once a week with bioluminescence imaging performed using the IVIS 100 (Xenogen) preclinical imaging system. Images were acquired 15 minutes following intraperitoneal injection with 150 mg/kg of D-luciferin (Gold Technology #LUCK-100). Display and adjustment of bioluminescence intensities were performed using Living Image 4.5.4 software (Perkin Elmer), and the luminescence scale is indicated in the figures.

In vivo analysis of a tumor-infiltrating SbCAR phenotype

Tumors from mice treated with the constitutive and inducible SbCAR were harvested at day 75 into RPMI (n = 3 per group) and were then minced by razor blade and digested for an hour in RPMI with an enzyme mixture from a human Tumor Dissociation Kit (Miltenyi Biotec #130-095-929) in a tumor gentleMACS Dissociator at 37°C to obtain single-cell suspensions. After incubation, the digested tumors were passed over a 70-μm cell strainer, and the tumor cells were collected by centrifugation. The cells were then washed with PBS and stained with a Live/Dead Zombie UV dye (BioLegend #423107) for 30 minutes. After that, cells were stained with anti–CD3 allophycocyanin-eFluor 780 (eBioscience 47-0036-42) to analyze the tumor-infiltrating T cells, with PE-Cy7 anti-PD-1 (clone EH12.1, 561272, BD Biosciences, RRID: AB_10611585), BV785 anti-TIM3 (clone F38-2E2, 345031, BioLegend, RRID: AB_2565832), and AF700 anti-LAG3 (clone 3DS223H, 56-2239-42, Thermo Fisher Scientific, RRID: AB_2688180) for T-cell exhaustion. Exhaustion and expression of mCherry (CAR induction) were assessed in the $CD3^+$ T-cell populations with LSRFortessa (BD Biosciences), and the analysis was performed in FlowJo software (TreeStar, RRID: SCR_008520).

Data availability

All raw data and reagents are available upon request from the corresponding author.

Results

To establish a novel toolkit of binders for CAR T-cell therapy, we focused on a set of tumor-associated surface antigens that are prevalently overexpressed in solid tumors, with a particular emphasis on ovarian cancer due to its well-documented antigen profile and therapeutic need. Utilizing a bacteriophage library that displays engineered human NPHP1 SH3 domains (sherpabodies hereafter), comprising roughly 10^{11} unique sequences, we conducted affinity screening against the extracellular domain of six recombinant TAAs expressed in 293T cells, namely, HER2, FOLR1, EpCAM, HER3, TROP2, and EphA2. These proteins are well-established targets in solid cancer immunotherapy (26, 27).

Successive rounds of biopanning, a method used to select phages with specific affinity for target antigens, yielded robust enrichment of phage clones for these six TAAs (**Fig. 1B**). From this enrichment, 1,152 individual phage clones were isolated after the third and fourth rounds of selection, confirmed to bind to their cognate protein, and subjected to DNA sequencing. This process resulted in the identification of 103 different sherpabodies, i.e., TAA-targeted NPHP1 SH3 domain derivatives with unique RT and n-src loop sequence signatures. We tested the relative binding strength of these candidates, using a phage-ELISA, and selected 20 sherpabodies with favorable affinities for further specificity testing (**Fig. 1C**). These tests confirmed that our selected sherpabodies bound exclusively to their intended target among the panel of six cancer-associated proteins (**Fig. 1D**). To have a more accurate determination of these sherpabody binding affinities (K_D), we used biolayer interferometry and measured the K_D of sherpabody clones 1205, 1322, and 1324, which target HER2, and found affinities ranging from 762 to 2,200 nanomolar (**Fig. 1E**).

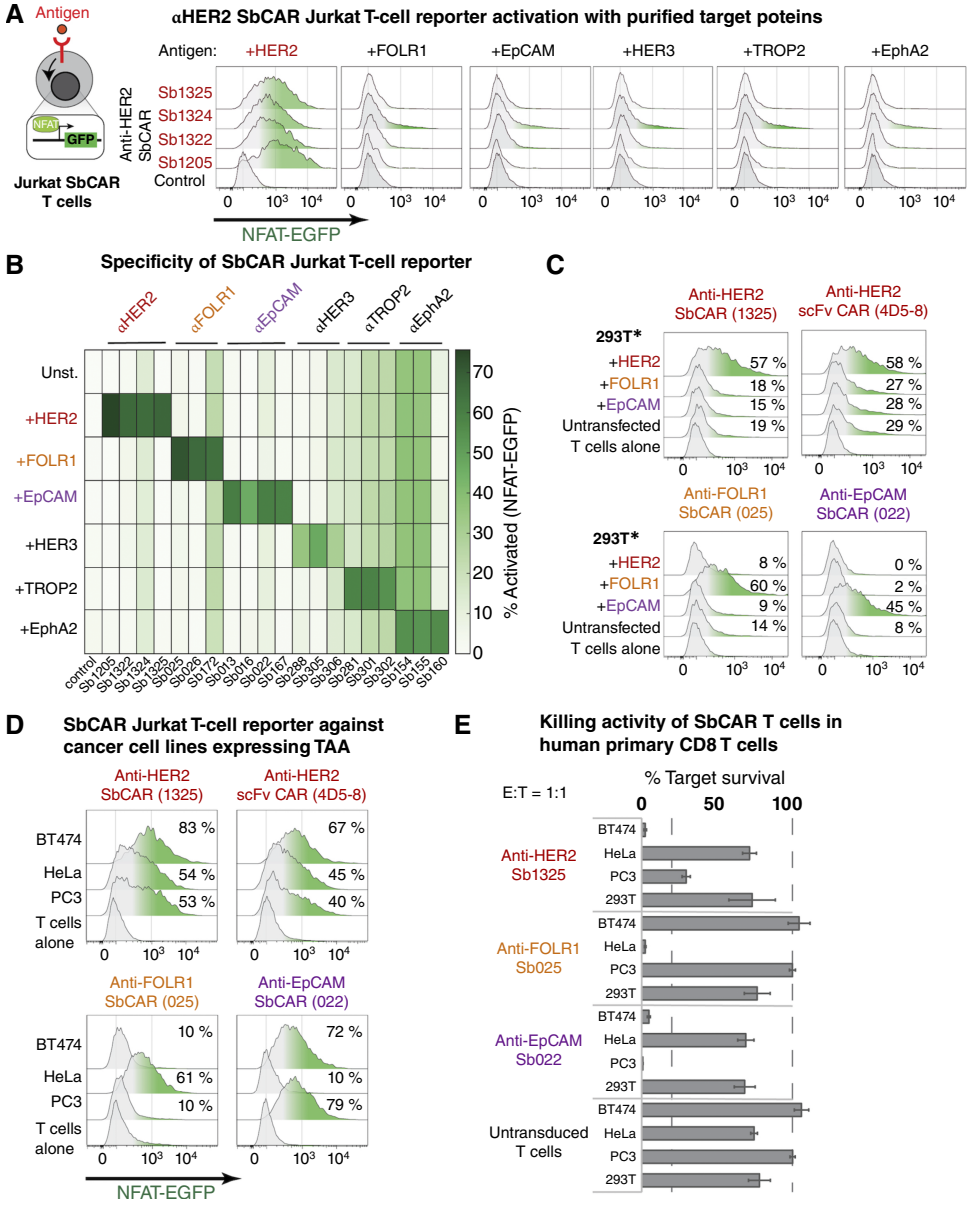

Figure 2.

In vitro activity of SbCAR constructs in Jurkat and human primary CD8 T cells. **A,** Schematic of the J76-TPR Jurkat T-cell–derived reporter line, which expresses a fluorescent protein under the control of T-cell activation–induced transcription factors. GFP controlled by the NFAT promoter is depicted. Representative flow cytometry distributions of GFP reporter for the J-CAR T cells engineered with anti-HER2 SbCARs and cultured with target proteins immobilized on cell culture plastic. **B,** Percentage of activated T cells as determined by GFP expression of J-CAR T cells engineered with SbCARs and cocultured with a panel of target proteins immobilized on cell culture plastic. The color scale has been adjusted to the maximum percentage of activated cells, and the percentage of activated T cells was calculated relative to the GFP fluorescence of a control SbCAR (Sb911) that does not target any antigen. Unst., unstimulated T cells. **C,** Representative FACS distributions for the GFP expression of J-CAR T cells reporter line engineered with SbCARs targeting the selected TAAs and cocultured with 293T* (HER2 K_D; see Supplementary Fig. S3) transfected with a panel of TAAs. The percentage of activated T cells is indicated and was calculated using T cells alone as a reference. **D,** Representative FACS distributions for GFP expression of J-CAR T cells reporter line engineered with SbCARs targeting the selected TAAs and cocultured with a panel of cancer cell lines (BT474, HeLa, and PC3). The percentage of activated T cells is indicated and was calculated using T cells alone as a reference. **E,** *In vitro* killing activity, measured by target cell bioluminescence, for human primary $CD8^+$ T cells engineered with indicated SbCARs and cocultured with a panel of cancer cell lines. Data are shown as percentage target survival, with bars indicating the mean and SEM ($n = 3$) at a 1:1 E:T ratio.

Importantly, the specificity of these sherpabodies extends to highly homologous proteins within the ErbB family. This characteristic is crucial for therapeutic applications given the family's role in various cellular processes and cancers (28). None of the sherpabodies targeting HER2 (ErbB2) and HER3 (ErbB3) showed cross-reactivity with EGFR (ErbB1), despite the extracellular domains

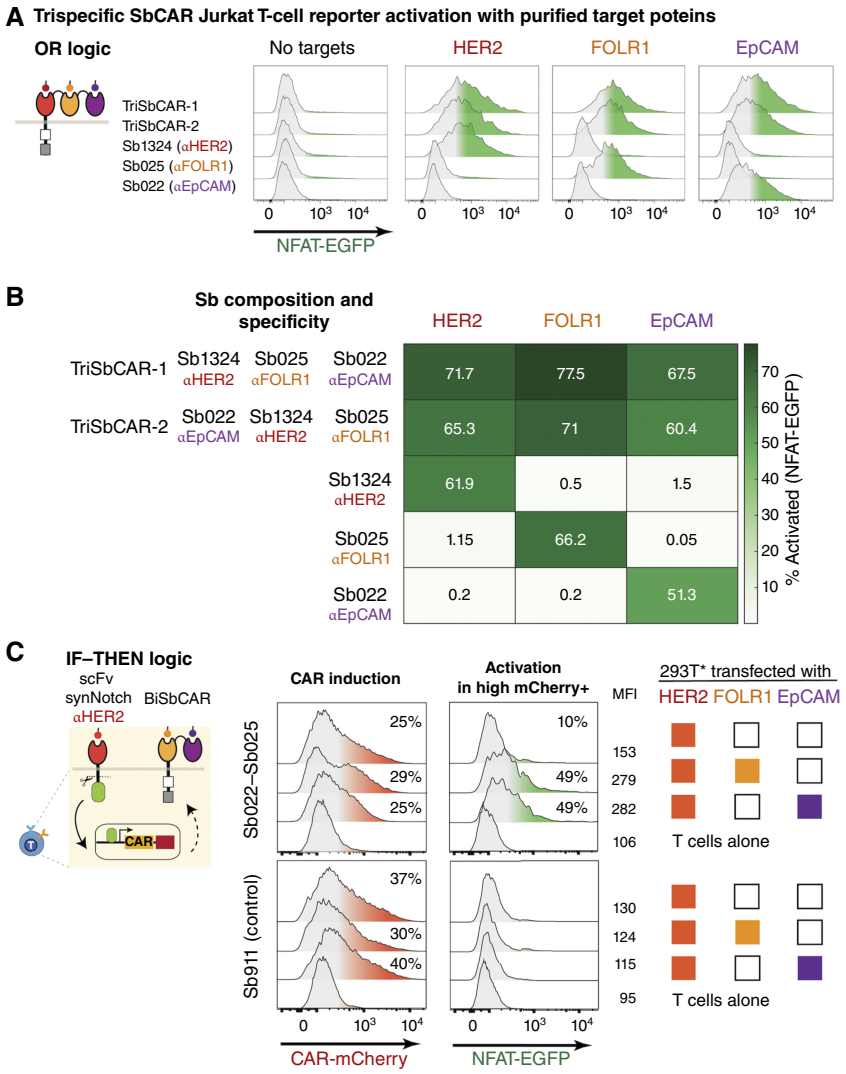

Figure 3.

Activation of multispecific SbCARs with OR and IF–THEN logic configurations. **A,** Schematic of a TriSbCAR with an OR logic configuration. Representative flow cytometry distributions of GFP reporter for the J-CAR T cells engineered with multispecific SbCARs and cultured with target proteins immobilized on cell culture plastic. The histograms are stacked by target protein. **B,** Percentage of activated T cells as determined by GFP expression driven by an NFAT promoter in J-CAR T cells. The composition and specificity for each TriSbCAR is indicated and color-coded by antigen. The percentage of activated T cells was calculated relative to the GFP fluorescence of SbCAR T cells without targets. The color scale was adjusted to the maximum percentage of activated cells. Sb, sherpabody. **C,** Schematic of a TriSbCAR with an IF–THEN logic configuration. A synNotch guided by an anti-HER2 scFv controls the expression of a BiSbCAR with an OR logic configuration. The BiSbCAR was fused to an mCherry fluorescent protein for detection. Jurkat T cells cocultured with 293T* (HER2 K_D) cells transfected with the indicated combination of TAAs. Representative flow cytometry distributions of mCherry expression and GFP expression driven by an NFAT promoter in J-CAR T cells. The corresponding CAR is indicated, with Sb022 to Sb025 shown at the top and control CAR (Sb911) shown at the bottom. The percentage of activated T cells was calculated relative to the mCherry fluorescence of T cells alone. The percentage of activated T cells was calculated from cells presenting high levels of mCherry signal. MFI, mean fluorescence intensity.

sharing approximately ~45% identity (28). Furthermore, a "sticky macromolecule" ELISA, designed to detect nonspecific interactions by including compounds known for promiscuous binding (19, 20), demonstrated that the selected sherpabodies did not exhibit polyreactive nonspecific binding (Supplementary Fig. S1), a critical attribute for therapeutic applications.

After confirming the specificity of the sherpabody set, we built second-generation CAR constructs by integrating the sherpabodies with the CD8 transmembrane domain and the intracellular domains of 4-1BB and CD3ζ. Additionally, we incorporated an mCherry fluorescent protein as a reporter for monitoring of construct expression. These SbCARs were subsequently cloned into a lentiviral vector to assess their functionality by transduction into the J76-TPR Jurkat T-cell–derived reporter line, which expresses three fluorescent proteins under the control of T-cell activation–induced transcription factors NFAT, NF-κB, or AP-1 (24). We hereafter refer to the Jurkat-derived J76-TPR reporter cells expressing our SbCAR constructs as J-CAR T cells, leveraging this system to study T-cell activation responses.

The functional capacity of the J-CAR T cells was first evaluated by monitoring T-cell activation upon exposure to target proteins immobilized on cell culture plastic. Notably, anti-HER2 J-CAR T cells selectively expressed GFP under the control of the NFAT reporter when presented with immobilized HER2 protein (**Fig. 2A**). This specific activation did not occur with the other TAAs, thus mirroring the target specificity previously demonstrated in the ELISA binding assays (**Fig. 1D**). This specificity was also consistently observed across several SbCARs targeting other TAAs (**Fig. 2B**). The observed correlation between binding specificity across the ELISA measurements (**Fig. 1D**) and antigen-induced T-cell activation as measured by the NFAT (**Fig. 2B**) and NF-κB (Supplementary Fig. S2) reporters highlights the potential of these engineered T cells to maintain target specificity in a cellular context.

We further evaluated the SbCAR functionality and specificity by displaying antigens on the surface of 293T* cells (which are HER2 negative derived using shRNA knockdown; Supplementary Fig. S3A) that were transfected with HER2, EpCAM, or FOLR1, as well as a panel of relevant human cancer cell lines (BT474, HeLa, and PC3—**Fig. 2D**) expressing various levels of these antigens (Supplementary Fig. S3B). For these studies, we selected a small set of promising candidates: Sb1205, Sb1324, and Sb1325 targeting

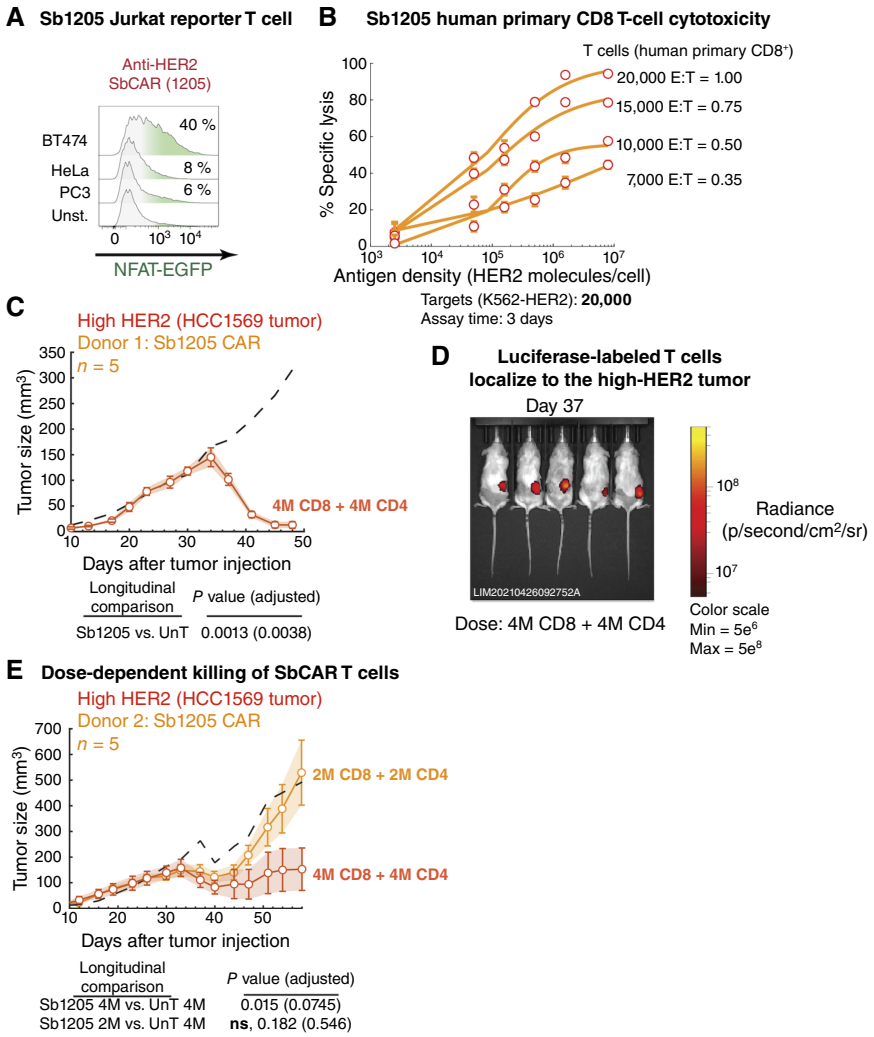

Figure 4.

In vitro and *in vivo* characterization of Sb1205 anti-HER2 CAR. **A,** Representative FACS distributions showing the EGFP fluorescence driven by an NFAT promoter in J-CAR T cells engineered with Sb1205 anti-HER2 CAR and cocultured with a panel of cancer cell lines. The percentage of activated T cells was calculated relative to the GFP fluorescence of SbCAR T cells alone (Unst., unstimulated T cells). **B,** *In vitro* cell killing curves as a function of target cell antigen density, using human primary CD8$^+$ T cells expressing a constitutive Sb1205 anti-HER2 CAR. Four different E:T ratios are shown. A total of 20,000 target cells were cocultured with (20,000, 15,000, 10,000, and 7,000) engineered T cells. The lines are drawn based on inspection. The percentage of specific lysis was determined using flow cytometry by counting the number of target cells after 3 days relative to a coculture of targets in the presence of untransduced T cells. Data are shown as the mean and SEM ($n = 3$). Target cells were K562 cells engineered to express different levels of HER2. **C,** Tumor volumes of breast cancer cells expressing high HER2 (HCC1569) after treatment with 8 million (4M CD8 + 4M CD4) T cells expressing an Sb1205 anti-HER2 CAR. The solid lines connect the means, and the error bars denote the SEM ($n = 5$). The black dashed line shows the tumor volumes after treatment with 8 million (4M CD8 + 4M CD4) untransduced T cells (UnT; see Supplementary Fig. S9 for details of control experiment). Three million target cells were inoculated into the flanks of NOD/SCID gamma mice, and T cells were transferred 28 days after tumor inoculation. **D,** Representative image of luciferase signal 9 days after T-cell injection in tumor-bearing mice treated with Sb1205 CAR T cells transduced with a luciferase reporter. Luciferase signal was only detected in the high HER2 tumor, indicating localized expansion ($n = 5$). **E,** Tumor volumes of breast cancer cells expressing high HER2 (HCC1569) after treatment with two different doses of T cells expressing an Sb1205 anti-HER2 CAR. The solid lines connect the means, and the error bars denote the SEM ($n = 5$). The black dashed line shows the tumor volumes after treatment with 8 million (4M CD8$^+$ and 4M CD4) untransduced T cells (see Supplementary Fig. S9 for details of control experiment). Three million target cells were inoculated into the flanks of NOD/SCID gamma mice, and T cells were transferred 28 days after tumor inoculation. Statistical longitudinal analyses were performed over entire segments of the tumor growth curves using TumGrowth (33). See Materials and Methods for more details. ns, not significant.

HER2; Sb022 targeting EpCAM; and Sb025 targeting FOLR1. These J-SbCAR T cells were cocultured with the TAA-transfected 293T* cells (**Fig. 2C**; Supplementary Fig. S3C) or the cancer cell lines (**Fig. 2D**), and the activation response was measured via flow cytometry.

The activation response of J-CAR T cells was consistent with the corresponding specificity of the SbCAR. Anti-HER2 CARs activated only in the presence of HER2-transfected 293T* and similarly for anti-FOLR1 and anti-EpCAM J-CAR T cells (**Fig. 2C**; Supplementary Fig. S3C). Furthermore, the anti-HER2

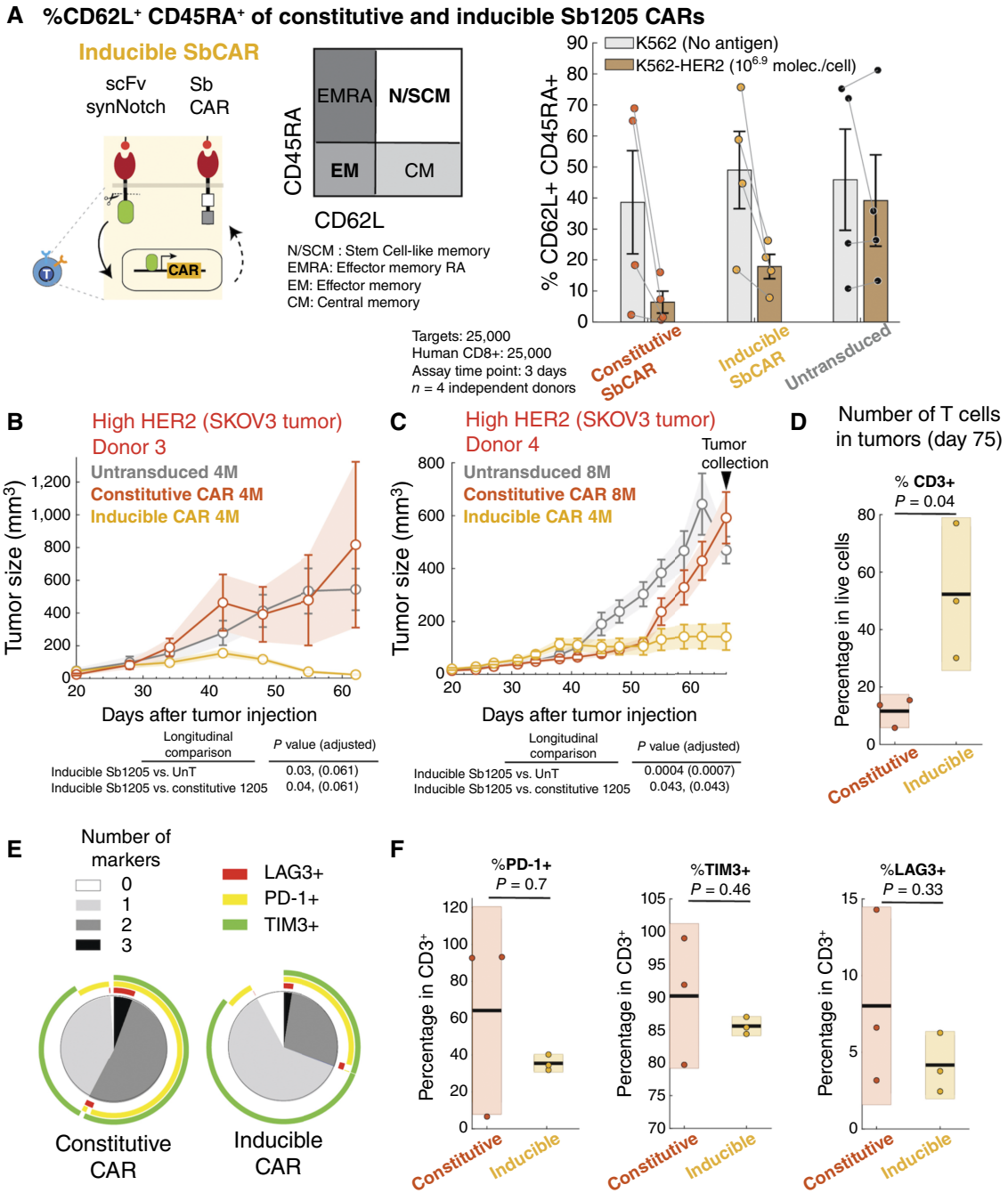

Figure 5.

In vitro and *in vivo* activities of constitutive and inducible Sb1205 anti-HER2 CARs. **A,** Schematic of a circuit for inducible expression of an SbCAR. An scFv-guided synNotch receptor is used to control the expression of an SbCAR. Differentiation phenotype of T cells based on CD45RA and CD62L markers. Percentage of $CD62L^{+}CD45RA^{+}$ T cells for constitutive and inducible Sb1205 CARs and untransduced T cells in cocultures with targets expressing the cognate antigen (HER2; $n = 4$ per group, four independent donor T cells). The bars show the average of measurements, and the bars indicate the SEM. The lines connect the corresponding measurements for each donor. CM, central memory; EM, effector memory; EMRA, effector memory RA; N/SCM, stem cell–like memory. **B,** Tumor volumes of ovarian cancer cells (SKOV3) after treatment with T cells expressing a constitutive (dark orange) or inducible (yellow) Sb1205 anti-HER2 CAR. The solid lines connect the means, and the error bars denote the SEM. The gray line shows the tumor volumes after treatment with untransduced T cells (UnT; see Supplementary Fig. S13 for details of individual animals $n = 6$–9). Three million high-HER2 ovarian cancer cells (SKOV3) were injected subcutaneously into the flanks of NOD/SCID gamma mice. Four million (2M CD8 + 2M CD4) engineered or untransduced human primary T cells were injected intravenously 37 days after tumor injection. **C,** Tumor volumes of ovarian cancer cells (SKOV3) after treatment with T cells expressing constitutive or inducible Sb1205 anti-HER2 CAR T cells from an additional donor. The solid lines connect the means, and the error bars denote the SEM. The gray line shows the tumor volumes after treatment with untransduced T cells. Three million high HER2 ovarian cancers (SKOV3) were injected subcutaneously in the flanks of (*Continued on the following page.*)

SbCAR (1325) induced GFP expression in J-CAR T cells when cocultured with cells expressing HER2 regardless of whether expression was high (BT474) or low (HeLa and PC3; **Fig. 2D**). This level of activation was comparable with that achieved by an anti-HER2 J-CAR T cell engineered with the scFv 4D5-8, derived from the antibody trastuzumab (22, 29), underscoring the potential of sherpabodies as alternatives to traditional scFvs. Moreover, the antigen-induced activation of SbCAR (1325) is robust and comparable with that of chemical stimulation of NFAT signaling using a combination of PMA and ionomycin (Supplementary Fig. S4).

Specificity in TAA targeting was evident as anti-FOLR1 J-CAR T cells and anti-EpCAM J-CAR T cells were activated by their respective antigens, with the former activating with FOLR1-expressing HeLa (cervical cancer) cells and the latter with EpCAM-expressing BT474 (breast cancer) and PC3 (prostate cancer) cells. Control J-CAR T cells, either untransduced or engineered with an inert sherpabody construct (Sb911), i.e., a wild-type human NPHP1 SH3 domain, did not exhibit activation (**Fig. 2D**). These findings support that SbCARs are capable of eliciting specific T-cell activation in response to their cognate TAAs found on various human cancer cell lines.

Next, we evaluated cytotoxic activity and cytokine secretion of human primary CD8 T cells engineered with the selected HER2-, EpCAM-, and FOLR1-targeting SbCARs. We modified BT474, PC3, HeLa, and 293T cell lines to stably express firefly luciferase, enabling us to monitor and quantify target cell viability after coculture with the SbCAR T cells. These assays revealed that each cancer cell line was specifically killed by the T cells expressing the corresponding SbCAR, supporting the functional specificity of the engineered T cells (**Fig. 2E**). Sb1325 CAR T cells killed both PC3 and BT474 cells despite differences in antigen expression, Sb025 CAR T cells killed HeLa cells, and Sb022 CAR T cells killed EpCAM-expressing cells BT474 and PC3. The observed cytotoxic effects exhibited clear dose-dependency according to the E:T cell ratio (Supplementary Fig. S5). As expected, untransduced T cells did not exhibit notable cytotoxicity against the panel of cancer cell lines.

Consistently, we observed robust secretion of IL2 and IFNγ by human primary SbCAR T cells cocultured with different cancer cell lines that strictly correlated with their cognate TAA expression (Supplementary Fig. S6). Given that PC3 and HeLa cell lines express low levels of HER2, we used for these assays PC3* and HeLa* (HER2-knockdown derivatives; Supplementary Fig. S3A) that were generated with shRNA similarly to 293T*. Altogether, these results support the utility and specificity of sherpabodies as targeting binding units for CARs in human primary T cells.

Building on the promising results of antigen-specific T-cell activation and cytotoxicity and to make use of compact nature and modularity of the sherpabody domains, we investigated the potential of sherpabodies to create multispecific T-cell receptors. We and others have shown that these could be valuable for increasing the specificity of tumor targeting against solid tumors (6, 10, 30–32). We sought to engineer T cells with OR and IF–THEN logic configurations as we have previously shown that these could be useful for targeting tumor heterogeneity. Thus, we first aimed to engineer multifunctional SbCARs with the capacity to engage three TAAs—HER2, FOLR1, and EpCAM in an "OR gate" configuration, which permits T-cell activation upon the presence of any single targeted antigen. In a proof-of-concept experiment, we constructed two trispecific SbCARs incorporating anti-HER2 (Sb1324), anti-FOLR1 (Sb025), and anti-EpCAM (Sb022) sherpabodies into two distinct configurations. We engineered the corresponding J-CAR reporter lines and cocultured them with the selected target proteins immobilized on cell culture plastic. Both trispecific SbCARs (TriSbCAR) triggered robust GFP expression against all three TAAs, indicating T-cell activation (**Fig. 3A** and **B**). This response was similar or even stronger than that of the monospecific SbCARs. Furthermore, a similar behavior was observed against the panel of cancer cell lines (Supplementary Fig. S7). Importantly, neither of the TriSbCARs exhibited antigen-independent activation (**Fig. 3A** and **B**; Supplementary Fig. S7).

Next, we constructed a trispecific CAR in an IF–THEN configuration. Specifically, we designed a system in which a previously characterized anti-HER2 synNotch receptor containing a variant of the 4D5 scFv (22) regulates the expression of a bispecific SbCAR designed with an OR-gated logic using anti-FOLR1 (Sb025) and anti-EpCAM (Sb022) sherpabodies (**Fig. 3C**). As intended, cocultures of J-CAR T cells bearing this circuit with HER2-transfected 293T induced the expression of mCherry-fused anti-FOLR1/EpCAM-BiSbCAR similarly to when we used a circuit that controls expression of a nontargeting SbCAR (Sb911). However, when and only when FOLR1 or EpCAM was expressed together with HER2, transfected 293T* triggered NFAT-induced GFP activation in J-CAR T cells transduced with this synNotch-BiSbCAR circuit. In contrast, anti–HER2-synNotch–induced expression of the control Sb911-CAR had no such effect. These results support the concept of sherpabody modularity and their potential to be integrated into multispecific CARs and circuits that combine IF–THEN–gated and OR-gated T-cell activation logic configurations for increasing the specificity of tumor 2targeting.

To assess the efficacy of SbCARs in a xenograft mouse model, we decided to focus on an anti-HER2 (Sb1205) construct. Sb1205 demonstrated robust specificity and good affinity (K_D = 762 nmol/L; **Fig. 1E**) as a soluble binder. We found specific activation of Sb1205-guided J-CAR T cells against purified target proteins (**Fig. 2A**) and in cocultures with 293T cells expressing transfected TAA proteins (Supplementary Fig. S3C). This behavior was also observed for J-CAR T cells in cocultures with the BT474, HeLa, and PC3 cancer cell lines (**Fig. 4A**). Human primary CD8 T cells expressing Sb1205 CAR showed a dose-dependent cytotoxic activity against various engineered target cells (K562 cell line) expressing different HER2 densities (**Fig. 4B**).

We established xenografts by administering HCC1569 breast cancer cells, which express high levels of HER2, into the flank of

(*Continued*.) NOD/SCID gamma mice. Eight million (4M CD8 + 4M CD4) untransduced or constitutive Sb1205 anti-HER2 CAR human primary T cells or 4 million (2M CD8 + 2M CD4) inducible Sb1205 anti-HER2 CAR were injected intravenously 37 days after tumor injection. The black arrow indicates the time (day 75) when tumors from the constitutive and inducible SbCAR T cells were collected. Statistical longitudinal analyses were performed over entire segments of the tumor growth curves using TumGrowth. **D,** Percentage of $CD3^+$ T cells in tumors collected 75 days after implantation (n = 3) from mice treated with constitutive or inducible Sb1205 CAR T cells. **E,** Expression of exhaustion markers on constitutive CAR and inducible Sb1205 CAR T cells collected 75 days after tumor injection. Pie chart shows the percentage of cells that express 0, 1, 2, or 3 exhaustion markers (PD-1, LAG3, or TIM3), average of three different tumors. Arc length shows the percentage of the indicated marker in each population. **F,** Percentage of cells expressing the exhaustion markers (PD-1, LAG3, or TIM3) on T cells collected from tumors 75 days after implantation.

NOD/SCID gamma mice. Concurrently, to serve as a comparative measure, we implanted PC3 prostate cancer cells, characterized by a low HER2 expression, on the contralateral side (Supplementary Fig. S9A). After establishing the tumors, we injected intravenously equal amounts of $CD4^+$ and $CD8^+$ human primary T cells transduced with the anti-HER2 SbCAR (Sb1205) and monitored tumor progression through caliper measurements (33).

A dose of 4M $CD8^+$ and 4M $CD4^+$ led to complete regression of the high HER2-expressing tumors (**Fig. 4C**). In contrast, the low HER2-expressing tumors grew at rates comparable with those observed with untransduced T cells (Supplementary Fig. S9B). This observation was supported by the localization and proliferation patterns of SbCAR T cells within the high-HER2 tumor, as observed by a cotransduced luciferase reporter (**Fig. 4D**; Supplementary Fig. S10). A robust cytotoxic response was further validated using T cells from a different donor (**Fig. 4E**; Supplementary Fig. S9D). However, we observed a dose-dependent cytotoxic effect, in which lowering the dose of SbCAR T cells by half (2M $CD8^+$ and 2M $CD4^+$) only resulted in delayed tumor growth, suggesting a threshold of T-cell quantity for effective tumor control (Supplementary Fig. S9D). Importantly, a comparable dose-dependent cytotoxic activity was observed *in vitro* and *in vivo* when using T cells engineered with a CAR derived from a low-affinity 4D5 scFv ($K_D = 3{,}910$ nmol/L; Supplementary Fig. S8; ref. 23). We conclude that SbCAR T cells show efficient and dose-dependent killing activity in xenograft mouse models.

Having demonstrated *in vitro* that SbCARs are suitable for building multispecific CARs and regulatory circuits, we wished to test the function of one of such circuits in a xenograft model. Previously, we showed that a circuit in which a synNotch receptor controls CAR expression can be used to optimize the antigen density threshold of T-cell activation to target only high antigen density target cells (22). To exploit the small size and modularity of sherpabodies for constructing such antigen density–sensing circuits, we designed a system in which an anti-HER2-synNotch receptor regulates the expression of anti-HER2 SbCAR (Sb1205), which we have termed "inducible SbCAR." We compared this system with the constitutive SbCAR (Sb1205) and a constitutive low-affinity scFv anti-HER2 CAR in cocultures with high HER2-expressing target cells (engineered K562-HER2 line). Specifically, we assessed the percentage of $CD45RA^+CD62L^+$ in T cells using flow cytometry (**Fig. 5A**; Supplementary Figs. S11 and S12), as the fraction of "stem cell–like memory" cells has been shown to correlate with *in vivo* expansion, persistence, and antitumor efficacy (34).

A repeated measures ANOVA test showed that these T cells are different in a "stem cell–like memory" phenotype ($CD62L^+CD45RA^+$) across four different donors (Supplementary Fig. S12). The inducible SbCAR group displays a unique profile, showing a significant difference compared with scFv-based CAR under both conditions (K562 and K562-HER2) and a significant difference with constitutive SbCAR under the no-antigen condition. There was a consistent decline in $CD62L^+CD45RA^+$ percentages from K562 to K562-HER2 coculture conditions for all engineered T cells, consistent with the antigen-induced functional shifts due to differentiation, suggesting that the inducible SbCAR could represent a functional phenotype balancing stem cell–like and activation phenotypes. This observation is consistent with other synNotch-induced CAR T cells targeting other antigens (9, 10).

To validate the potential advantages of this phenotype, we conducted a series of *in vivo* experiments using two HER2-expressing tumor models, SKOV3 (ovarian cancer) and HCC1569 (breast cancer), with engineered T cells from two distinct donors. The inducible SbCAR consistently surpassed the performance of the constitutive SbCAR in its antitumor activity in both tumor models (**Fig. 5B** and **C**; Supplementary Figs. S13 and S14). In an analysis of three of nine SKOV3 tumors at 75 days after tumor inoculation, we identified a higher presence of $CD3^+$ T cells for the inducible CAR group compared with the constitutive group (**Fig. 5D**). Importantly, these were the tumors that escaped T-cell control as most tumors treated with the inducible SbCAR (6/9) were eradicated using a lower T-cell dose than that required for the constitutive sherpabody CAR T cells (Supplementary Fig. S10).

Further analysis of the tumor-infiltrating T cells via a panel of markers correlating with exhaustion (PD-1, LAG3, and TIM3) revealed that a greater fraction of constitutive SbCAR T cells expressed one or more of these markers, compared with inducible SbCAR T cells. The level of expression of each marker was higher but not significant in the constitutive SbCAR group compared with the inducible group (**Fig. 5E** and **F**). Interestingly, the expression level of SbCAR on the T cells in the inducible group was lower than that in the constitutive group (Supplementary Fig. S15), suggesting that a lower expression level of SbCAR could be a cause of mitigating T-cell exhaustion. Overall, these findings support that inducible SbCAR expression, mediated by the synNotch circuit, results in enhanced persistence and antitumor activity in xenograft mouse models when compared with constitutive expression of CARs. This strategy may offer a path to more durable CAR T-cell therapies by controlling a state in which T cells retain their functional capacity over extended periods.

Discussion

The success of engineered T-cell therapies in blood cancers has opened new opportunities in the battle against cancer, especially many solid tumors that have remained difficult to treat. Our study presents sherpabodies as a promising and versatile antigen recognition platform for engineered T-cell therapies, demonstrating specificity and efficacy in targeting TAAs commonly overexpressed in such cancers.

We successfully identified a large collection of promising sherpabodies specific for a panel of solid cancer TAAs through just a few rounds of biopanning of a semisynthetic phage display library, highlighting the targeting capacity of sherpabodies and the flexibility of this platform. Importantly, we noted no cross-reactivity of sherpabodies within closely related proteins, a critical factor in mitigating potential off-tumor toxicity.

In our functional assays, SbCARs showed potent activation and cytotoxicity *in vitro*. Notably, the anti-HER2 SbCARs (Sb1324, Sb1325, and Sb1205) exhibited activation across various HER2 expression levels, suggesting a capacity for effective targeting in heterogeneous tumor environments. This efficacy parallels the well-characterized anti-HER2 scFv 4D5-8, underlining the potential of sherpabodies as a viable alternative to traditional scFvs.

Our exploration into the construction of multispecific CARs using sherpabodies in OR and IF–THEN logic configurations highlights the potential of this platform. The multispecific OR-gated TriSbCARs induced robust T-cell activation profiles that correlated with the TAA expression patterns and matched or even surpassed the activity of the monospecific SbCARs. Although coexpression of multiple TAAs in the target cells may help by increasing the total TAA density on the surface of these cells, no apparent synergy in targeting cells with expression of multiple TAAs was observed, and due to spatial constraints, it is unlikely that the individual

sherpabody modules within a single TriSbCAR could simultaneously engage with their cognate targets. The minor differences in the activation potential of the two TriSbCARs tested indicated that the relative positioning of the sherpabody modules is not critical but a variable that should be considered and might be more important for other set of target antigens.

Together with the specificity behavior obtained with the IF–THEN logic circuits, these results showcase the concept of sherpabody modularity and their potential to be integrated into more complex, yet highly specific, antigen recognition strategies. Importantly, multiantigen recognition circuits have been shown to enhance the specificity of tumor targeting to avoid off-tumor toxicity or to deal with cases of tumor heterogeneity. For example, we previously showed a circuit for cell therapies against glioblastoma. A synNotch receptor that targets a tumor-specific signal such as EGFRVIII induces expression of a bivalent CAR-targeting IL13-Rα2 and EphA2. This strategy could be powerful to overcome tumor heterogeneity and exhaustion in the context of glioblastoma (10). Here, we showed that sherpabodies are compatible with these designs and potentially useful for engineering even more complex circuit architectures.

The *in vivo* results from the xenograft mouse models with anti-HER2 SbCARs correlated with the *in vitro* findings, with a robust, albeit dose-dependent, regression of two high HER2-expressing tumor models (ovarian and breast cancers). The variable responses at different T-cell dosages emphasize the importance of dose optimization for clinical translation.

Our synthetic circuit employing a synNotch-controlled inducible SbCAR T-cell system represents a promising advancement to enhance the performance of tumor-targeting T cells. This configuration displayed a larger fraction of "stem cell–like memory" phenotype *in vitro*, which correlated with improved antitumor efficacy. Indeed, the inducible SbCAR T cells outperformed the constitutive SbCAR both in eradicating tumor and in maintaining a larger fraction of T cells in the tumor over time *in vivo* across two high HER2-expressing tumor models, thus showing enhanced T-cell persistence. This suggests that the inducible system may offer a solution to the challenge of T-cell persistence, a common obstacle in CAR T-cell therapy.

The small size of sherpabodies is another advantage for engineering T cells (**Fig. 6A**). Made of approximately 60 amino acids, sherpabodies are smaller than other non–scFv-binding modules recently reported and reviewed for CAR T-cell targeting (35). This characteristic ensures that the resulting receptor or circuit construct is more compact compared with those employing larger antibody fragments, potentially increasing the efficiency during manufacturing (**Fig. 6B**). CAR T cells used for cancer therapy are usually generated via *in vitro* transduction of the desired CAR construct into patient's immune cells using lentiviral vectors. The maximal size of genetic material that can be inserted in these vectors is approximately 9 kb, but smaller payloads usually have >100-fold higher titers. Furthermore, the infectivity of lentiviral vectors decreases linearly as the packaged payload size grows (36). As the complexity of the CAR constructs and circuits increases, it is therefore of critical importance to minimize the size of every component used to design these systems.

Additionally, sherpabodies have an affinity in the nanomolar/low-micromolar range that is inherently suited for effective cellular targeting without the risk of binding too tightly—a phenomenon that can trigger rapid receptor internalization or capturing of the target antigen from the target cell surface, leading to diminished therapeutic efficacy. Although the affinity of conventional antibodies can be engineered downward to avoid such pitfalls, achieving this delicate balance often proves challenging and risks compromising specificity. In contrast, sherpabodies can be selected for optimal affinity without such trade-offs, making them not only a pragmatic choice but also a potentially more effective one in the design of CAR T-cell therapies.

Finally, an outstanding feature of sherpabodies for molecular targeting is their inherent modularity. They enable the construction of complex, multivalent receptors and regulatory circuits that could be tailored for precision oncology. This modularity is not only a structural feature; it is a functional dial that allows for the combination of different targeting units within a single receptor or as a part of a circuit, providing a versatile platform for potentially addressing the heterogeneity of tumor antigens and persistence in the tumor microenvironment (**Fig. 6C**). Indeed, in nature, the SH3 fold is frequently used for multimodular target protein recognition, and a single protein can contain as many as six SH3 domains with different binding specificities (37).

Collectively, our findings support the utility of sherpabodies as a modular and adaptable platform for antigen recognition in T-cell engineering. This study lays the groundwork for the development of a new class of receptors for cell therapies, potentially offering more

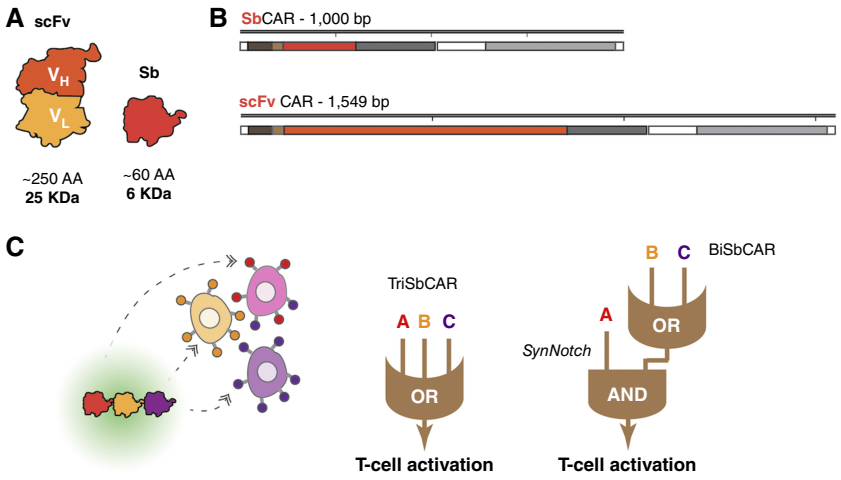

Figure 6.
Sherpabodies can serve as a versatile recognition platform for engineered T cells. **A,** Schematic and size comparison of an scFv and a sherpabody (Sb). **B,** Construct design for sherpabody-based and scFv-based CARs. Sherpabodies are compact and can save up to a third of genetic payload in a CAR construct. **C,** Schematic of a multispecific sherpabody-based trimeric recognition domain and multispecific receptors and circuits for OR and IF–THEN logic gated SbCARs showcased in this study.

targeted, persistent, and safer options for treating a range of solid tumors. Further exploration into the use of sherpabodies and inducible SbCAR systems will be required to understand the mechanistic basis of the superior antitumor activity, which may lead to significant improvements in the efficacy and durability of T-cell therapies for patients with cancer. We speculate that this phenotype is the result of whole-scale remodeling of the exhaustion-associated epigenome as previously described for studies with small molecules and transient resting of CAR T cells (38). Future studies should focus on understanding and further exploring the opportunities provided by the modularity of the sherpabody platform, optimizing dosing strategies, and expanding the range of TAAs targeted by these engineered T cells, as well as expanding combinatorial receptor designs.

The clinical potential of sherpabodies in CAR T-cell therapy is promising, yet translating these findings into human trials will require rigorous validation of safety and efficacy. Our research indicates that sherpabodies can be tailored for specificity and persistence, which are critical for clinical success. The inducible SbCAR system, which controls the CAR expression level, may represent an advantage in overcoming the limitations of current CAR T-cell therapies, such as T-cell persistence and the maintenance of long-term antitumor activity.

In conclusion, our study provides compelling evidence that sherpabodies can serve as a versatile antigen recognition platform for engineered T cells. By harnessing the compact, stable, and modular nature of sherpabodies, we can create SbCARs that are potentially a new addition for the treatment of solid tumors. Our inducible CAR circuit system further enhances the therapeutic potential of T-cell therapies, offering a strategy to improve the persistence and effectiveness of CAR T cells in clinical settings.

Authors' Disclosures

R.A. Hernández-López reports grants from Burroughs Wellcome Fund and Cancer Research Institute during the conduct of the study. P.M. Ojala reports grants from Sigrid Juselius Foundation, Cancer Foundation Finland, and Finnish Red Cross Blood Center Research Foundation during the conduct of the study. W.A. Lim reports grants from NIH during the conduct of the study, as well as other support from Gilead Sciences, Intellia Therapeutics, Allogene Therapeutics, and Burroughs Wellcome Fund outside the submitted work. K. Saksela reports grants from Research Council of Finland and Cancer Foundation Finland during the conduct of the study; a patent for sherpabodies (WO2017009533) issued; and being a founder and shareholder of Next Biomed Therapies Oy, which develops sherpabody-based targeting technologies. No disclosures were reported by the other authors.

Authors' Contributions

R.A. Hernández-López: Conceptualization, resources, data curation, formal analysis, validation, investigation, visualization, methodology, writing–original draft, writing–review and editing. **T. Kesti:** Data curation, formal analysis, investigation, visualization, methodology, writing–review and editing. **A.R. Mäkelä:** Resources, data curation, formal analysis, validation, investigation, visualization, methodology, writing–review and editing. **Z. Zhao:** Investigation. **W. Yu:** Investigation. **Y. Tonai:** Investigation. **H.J. Monzo:** Formal analysis, investigation, methodology, writing–review and editing. **K. Kalander:** Investigation. **S. Leppä:** Supervision, project administration, writing–review and editing. **P.M. Ojala:** Conceptualization, formal analysis, supervision, project administration, writing–review and editing. **W.A. Lim:** Conceptualization, resources, supervision, funding acquisition, project administration, writing–review and editing. **K. Saksela:** Conceptualization, resources, formal analysis, supervision, funding acquisition, validation, methodology, writing–original draft, project administration, writing–review and editing.

Acknowledgments

We thank members of the W.A. Lim and K. Saksela labs for advice and helpful discussions. We thank Matti Korhonen, Manar Elmadani, and the remaining members of the iCell group at the Finnish Red Cross Blood Service for advice and assistance with human T-cell isolation and manipulation. We thank the HiLIFE flow cytometry unit at the University of Helsinki and the Biocenter Oulu biophysical protein analysis core facility and the members of Biocenter Finland for use of facilities and their expertise, respectively. This work was supported by Research Council of Finland grants 331787 and 365346 and Cancer Foundation Finland grant 230119 (K. Saksela) and NIH grants R01CA220257, U54CA244438, and U01CA265697 (W.A. Lim). R.A. Hernández-López was a Cancer Research Institute Irvington Fellow supported by the Cancer Research Institute and holds a Career Award at the Scientific Interface from the Burroughs Wellcome Fund.

Note

Supplementary data for this article are available at Cancer Research Online (http://cancerres.aacrjournals.org/).

Received June 11, 2024; revised November 23, 2024; accepted February 24, 2025; posted first March 3, 2025.

References

1. Labanieh L, Mackall CL. CAR immune cells: design principles, resistance and the next generation. Nature 2023;614:635–48.
2. Khan AN, Asija S, Pendhari J, Purwar R. CAR-T cell therapy in hematological malignancies: where are we now and where are we heading for? Eur J Haematol 2024;112:6–18.
3. Cappell KM, Kochenderfer JN. Long-term outcomes following CAR T cell therapy: what we know so far. Nat Rev Clin Oncol 2023;20:359–71.
4. Flugel CL, Majzner RG, Krenciute G, Dotti G, Riddell SR, Wagner DL, et al. Overcoming on-target, off-tumour toxicity of CAR T cell therapy for solid tumours. Nat Rev Clin Oncol 2023;20:49–62.
5. Dannenfelser R, Allen GM, VanderSluis B, Koegel AK, Levinson S, Stark SR, et al. Discriminatory power of combinatorial antigen recognition in cancer T cell therapies. Cell Syst 2020;11:215–28.e5.
6. Williams JZ, Allen GM, Shah D, Sterin IS, Kim KH, Garcia VP, et al. Precise T cell recognition programs designed by transcriptionally linking multiple receptors. Science 2020;370:1099–104.
7. Cho JH, Okuma A, Sofjan K, Lee S, Collins JJ, Wong WW. Engineering advanced logic and distributed computing in human CAR immune cells. Nat Commun 2021 12:792.
8. Roybal KT, Rupp LJ, Morsut L, Walker WJ, McNally KA, Park JS, et al. Precision tumor recognition by T cells with combinatorial antigen-sensing circuits. Cell 2016;164:770–9.
9. Hyrenius-Wittsten A, Su Y, Park M, Garcia JM, Alavi J, Perry N, et al. SynNotch CAR circuits enhance solid tumor recognition and promote persistent antitumor activity in mouse models. Sci Transl Med 2021;13:eabd8836.
10. Choe JH, Watchmaker PB, Simic MS, Gilbert RD, Li AW, Krasnow NA, et al. SynNotch-CAR T cells overcome challenges of specificity, heterogeneity, and persistence in treating glioblastoma. Sci Transl Med 2021;13:eabe7378.
11. Hamers-Casterman C, Atarhouch T, Muyldermans S, Robinson G, Hamers C, Songa EB, et al. Naturally occurring antibodies devoid of light chains. Nature 1993;363:446–8.
12. Unciti-Broceta JD, Del Castillo T, Soriano M, Magez S, Garcia-Salcedo JA. Novel therapy based on camelid nanobodies. Ther Deliv 2013;4:1321–36.
13. Nasiri F, Safarzadeh Kozani P, Rahbarizadeh F. T-cells engineered with a novel VHH-based chimeric antigen receptor against CD19 exhibit comparable tumoricidal efficacy to their FMC63-based counterparts. Front Immunol 2023;14:1063838.
14. Xie YJ, Dougan M, Jailkhani N, Ingram J, Fang T, Kummer L, et al. Nanobody-based CAR T cells that target the tumor microenvironment inhibit the growth of solid tumors in immunocompetent mice. Proc Natl Acad Sci U S A 2019;116:7624–31.
15. Mäkelä AR, Uğurlu H, Hannula L, Kant R, Salminen P, Fagerlund R, et al. Intranasal trimeric sherpabody inhibits SARS-CoV-2 including recent immunoevasive Omicron subvariants. Nat Commun 2023;14:1637.

16. Silacci M, Lembke W, Woods R, Attinger-Toller I, Baenziger-Tobler N, Batey S, et al. Discovery and characterization of COVA322, a clinical-stage bispecific TNF/IL-17A inhibitor for the treatment of inflammatory diseases. MAbs 2016;8:141–9.
17. Hiipakka M, Poikonen K, Saksela K. SH3 domains with high affinity and engineered ligand specificities targeted to HIV-1 Nef. J Mol Biol 1999;293:1097–106.
18. Grabulovski D, Kaspar M, Neri D. A novel, non-immunogenic Fyn SH3-derived binding protein with tumor vascular targeting properties. J Biol Chem 2007;282:3196–204.
19. Jain T, Sun T, Durand S, Hall A, Houston NR, Nett JH, et al. Biophysical properties of the clinical-stage antibody landscape. Proc Natl Acad Sci U S A 2017;114:944–9.
20. Mouquet H, Scheid JF, Zoller MJ, Krogsgaard M, Ott RG, Shukair S, et al. Polyreactivity increases the apparent affinity of anti-HIV antibodies by heteroligation. Nature 2010;467:591–5.
21. Roybal KT, Williams JZ, Morsut L, Rupp LJ, Kolinko I, Choe JH, et al. Engineering T cells with customized therapeutic response programs using synthetic Notch receptors. Cell 2016;167:419–32.e16.
22. Hernandez-Lopez RA, Yu W, Cabral KA, Creasey OA, Lopez Pazmino MDP, Tonai Y, et al. T cell circuits that sense antigen density with an ultrasensitive threshold. Science 2021;371:1166–71.
23. Liu X, Jiang S, Fang C, Yang S, Olalere D, Pequignot EC, et al. Affinity-tuned ErbB2 or EGFR chimeric antigen receptor T cells exhibit an increased therapeutic index against tumors in mice. Cancer Res 2015;75:3596–607.
24. Rosskopf S, Leitner J, Paster W, Morton LT, Hagedoorn RS, Steinberger P, et al. A Jurkat 76 based triple parameter reporter system to evaluate TCR functions and adoptive T cell strategies. Oncotarget 2018;9:17608–19.
25. Monzo HJ, Kalander K, Hyytiäinen MM, Elbasani E, Wall J, Moyano-Galceran L, et al. Efficacy and safety of glycosphingolipid SSEA-4 targeting CAR-T cells in an ovarian carcinoma model. Mol Cancer Ther 2023;22:1319–31.
26. Maher J, Davies DM. CAR-based immunotherapy of solid tumours - a survey of the emerging targets. Cancers (Basel) 2023;15:1171.
27. Marofi F, Motavalli R, Safonov VA, Thangavelu L, Yumashev AV, Alexander M, et al. CAR T cells in solid tumors: challenges and opportunities. Stem Cell Res Ther 2021;12:81.
28. Sheng Q, Liu J. The therapeutic potential of targeting the EGFR family in epithelial ovarian cancer. Br J Cancer 2011;104:1241–5.
29. Carter P, Presta L, Gorman CM, Ridgway JB, Henner D, Wong WL, et al. Humanization of an anti-p185HER2 antibody for human cancer therapy. Proc Natl Acad Sci U S A 1992;89:4285–9.
30. Balakrishnan A, Rajan A, Salter AI, Kosasih PL, Wu Q, Voutsinas J, et al. Multispecific targeting with synthetic ankyrin repeat motif chimeric antigen receptors. Clin Cancer Res 2019;25:7506–16.
31. Schneider D, Xiong Y, Wu D, Hu P, Alabanza L, Steimle B, et al. Trispecific CD19-CD20-CD22-targeting duoCAR-T cells eliminate antigen-heterogeneous B cell tumors in preclinical models. Sci Transl Med 2021;13:eabc6401.
32. Schmidts A, Srivastava AA, Ramapriyan R, Bailey SR, Bouffard AA, Cahill DP, et al. Tandem chimeric antigen receptor (CAR) T cells targeting EGFRvIII and IL-13Rα2 are effective against heterogeneous glioblastoma. Neurooncol Adv 2023;5:vdac185.
33. Enot DP, Vacchelli E, Jacquelot N, Zitvogel L, Kroemer G. TumGrowth: an open-access web tool for the statistical analysis of tumor growth curves. Oncoimmunology 2018;7:e1462431.
34. Xu Y, Zhang M, Ramos CA, Durett A, Liu E, Dakhova O, et al. Closely related T-memory stem cells correlate with in vivo expansion of CAR.CD19-T cells and are preserved by IL-7 and IL-15. Blood 2014;123:3750–9.
35. Zajc CU, Salzer B, Taft JM, Reddy ST, Lehner M, Traxlmayr MW. Driving CARs with alternative navigation tools - the potential of engineered binding scaffolds. FEBS J 2021;288:2103–18.
36. Sweeney NP, Vink CA. The impact of lentiviral vector genome size and producer cell genomic to gag-pol mRNA ratios on packaging efficiency and titre. Mol Ther Methods Clin Dev 2021;21:574–84.
37. Salazar MA, Kwiatkowski AV, Pellegrini L, Cestra G, Butler MH, Rossman KL, et al. Tuba, a novel protein containing bin/amphiphysin/Rvs and Dbl homology domains, links dynamin to regulation of the actin cytoskeleton. J Biol Chem 2003;278:49031–43.
38. Weber EW, Parker KR, Sotillo E, Lynn RC, Anbunathan H, Lattin J, et al. Transient rest restores functionality in exhausted CAR-T cells through epigenetic remodeling. Science 2021;372:eaba1786.